Proceedings of the ASME 2011 International Manufacturing Science and Engineering Conference
MSEC2011
June 13-17, 2011, Corvallis, Oregon, USA

MSEC2011-50130

MODELING OF SEMI-SOLID POWDER PROCESSING FOR A CLOSED DIE COMPACTION

Yufeng Wu and Gap-Yong Kim[1]
Dept. of Mechanical Engineering, Iowa State University
Ames, Iowa, USA
[1]Contact Author

ABSTRACT

Semi-solid powder processing (SPP) is a promising technique in the fabrication of composite materials. Former work has experimentally shown that SPP was able to synthesize composite materials with reduced load and high efficiency. However, limited work was found in the modeling of the SPP. In this work, SPP was modeled with Shima-Oyane's model and compared with experimental data in a closed die compaction setup. The evolution and distribution of the density and stress were analyzed. The model prediction agreed with the experimentally measured values. As the compaction pressure increased, the density gradient in the axial compaction direction decreased, while the stress gradient increased.

INTRODUCTION

Semi-solid powder processing (SPP) combines the benefits of the semi-solid forming and powder metallurgy [1-3]. It is capable of tailoring the composite properties by controlling elemental powders or adding fibers [4-6]. It also eliminates post processing steps required in powder metallurgy routes. SPP has been applied to fabricate particle/fiber reinforced metal composite such as Al-SiC [7-11] and other alloy materials including Al-Ti [12, 13] and Al-Mg [14]. However, limited work has been done to model the process.

Several models have been developed to describe the powder compaction process at solid state and may be extended for the powder processing in the semi-solid range. Drucker-prager cap model is one of the most widely used powder compaction models [15]. It is capable of providing an accurate prediction of density evolution based on the pressure applied [16]. To determine the parameters used in this model, however, a triaxial compression experiment needs to be conducted, which is delicate and requires sophisticated equipment [15]. Fleck et al. [17] developed a yielding criterion of powder compacts based on the particle strain energy analysis, enabling a direct application of the constitutive equations to the powder compaction process. Nevertheless, the predicted flow stress could not fully capture the behavior of the soft powder compaction [18]. Shima and Oyane [19] proposed a yield criterion for compressible material. And the model had been successfully applied in both room temperature [19] and high temperature powder compactions [20].

In this work, Shima and Oyane's model was extended to predict the closed die powder compaction process. Al6061 powder was compacted in room temperature, and at elevated temperatures below the melting point (550°C) and in the semi-solid range (600°C). The evolution and distribution of density and stress were evaluated.

THEORETICAL BACKGROUND

Between the solidus and liquidus temperature, alloy material is partly melted, and therefore, both solid and liquid phases coexist. The liquid fraction of the material can be defined as:

$$f_l = \frac{V_l}{V_s + V_l} \tag{1}$$

where, f_l is the liquid fraction of the material; V_s and V_l are the volume of the solid and liquid phases, respectively.

The solid density refers to the relative density occupied by the solid phase material:

$$D_s = \frac{V_s}{V_s + V_l + V_p} \tag{2}$$

where, D_s is the solid density; and V_p is the volume of the pores. The relative density can be calculated as:

$$D = \frac{D_s}{1 - f_l} \tag{3}$$

The pressure applied to the powder compact can be divided into three parts [20]:

$$\sigma_{ij}{}^{t} = \sigma_{ij}{}^{s} f_s + \delta_{ij} p_l f_l + \delta_{ij} p_g g \tag{4}$$

where, $\sigma_{ij}{}^{t}$ is the total stress; $\sigma_{ij}{}^{s}$ is the stress tensor related to solid phase; δ_{ij} is Kronecker delta; p_l and p_g are the hydrostatic pressure of the liquid and pores; g is the porosity.

Typically, particles melt from the outer surface, which leaves the material with a solid core. Therefore, it was assumed that the behavior of the solid cores will follow that of the solid powder compact. The solid powder compact follows the yield criterion for compressible materials and can be represented as follows [19]:

$$f'\sigma_{eq} = \left\{ \frac{\left[(\sigma_{xx}-\sigma_{yy})^2 + (\sigma_{yy}-\sigma_{zz})^2 + (\sigma_{xx}-\sigma_{zz})^2\right]}{2} + \left(\frac{\sigma_m}{f}\right)^2 \right\}^{\frac{1}{2}} \quad (5)$$

where, σ_{eq} is the equivalent yield stress of the matrix material; σ_{xx}, σ_{yy}, and σ_{zz} are normal stresses to the powder compact in the x, y and z directions, respectively, and σ_{zz} is the stress parallel to the axis of the punch. $\sigma_{ii}= \sigma_{ii}^s f_s$; $\sigma_m=(\sigma_{xx}+\sigma_{yy}+\sigma_{zz})/3$; $f'=D_s^n$; $f=1/[a(1-D_s)^b]$. n, a and b are material related parameters, where n=2.4, a=2.0 and b=0.6 were used in the computation. For closed die compaction, Eqn. (5) can be further simplified as:

$$\sigma_{zz}/\sigma_{eq} = D_s^n \left(f^2 + \frac{4}{9}\right)^{\frac{1}{2}} \quad (6)$$

$$\varepsilon_{eq} = 0.633 D_s - 0.068 \ln(1-D_s) + \varepsilon_0 \quad (7)$$

where, ε_{eq} is the equivalent strain to the metal matrix material; ε_0 is an integration constant which is determined by substituting ε_{eq}=0 for D_s=D_{s0} (initial solid density). Equation (7) is applicable when particles form interconnected structure, which occurs when relative solid density, D_s, is higher than 0.6. When the particles are loosely stacked, the particles rearrange during compaction. The following strain-density relationship was proposed and applied when D_s <0.6:

$$\varepsilon_{eq} = 10(D_s - D_{s0})^3 \quad (8)$$

When the density is low, the liquid phase cannot take any external load due to the existing pores connected to the atmosphere. As the solid density increases, the liquid phase may become isolated from the atmosphere, and therefore, can undertake external pressure. When the liquid fraction is low, the hydrostatic pressure applied on the liquid phase, p_l, will then be equal to the pressure within the pores enclosed by the solid-liquid mixture, which can be estimated from [21]:

$$p_l = p_g = p_{ex} \frac{g_{cl}}{g} \frac{1-g}{1-g_{cl}} - p_{ex} \quad (9)$$

where, p_{ex} is the external gas pressure, in the current case it is atmospheric pressure; g_{cl} is the pore close porosity (typically, g_{cl}=0.125).

The density of the powder during compaction is also affected by the wall friction. When the aspect ratio of compact height to radius (H/R) is high, the powder-wall friction becomes significant and influences the density distribution in the axial direction. If H/R is larger than 2, the slab equilibrium theory holds, and the effect of the friction on the stress distribution follows [15]:

$$d\sigma_{zz}/\sigma_{zz} = \left(\frac{2\mu\alpha}{R}\right) dz \quad (10)$$

where, μ is the friction coefficient between the powder compact and the die wall; α is the stress transmission coefficient and $\alpha=\sigma_{yy}/\sigma_{zz}$ and can be evaluated with $\alpha=\nu/(1-\nu)$ in the current case; and R is the radius of the die. Therefore, Eqn. (10) enables estimation of the stress distribution along the axial direction. Friction conditions change with the existence of liquid phase. μ=0.24 was used for temperatures up to 550°C, and μ=0.14 was used at 600°C. ν is the Poisson's ratio and can be estimated by [19]:

$$\nu = \frac{0.5\left(1-\frac{2}{9f^2}\right)}{1+\frac{1}{9f^2}} \quad (11)$$

The material properties at various temperatures are different. At room temperature, the following equation was used to describe the flow stress of the matrix material [22]:

$$\sigma_{eq} = 224\varepsilon_{eq}^{0.209}\ MPa \quad (12)$$

In the range of 550–600°C, the flow stress is dependent on both the strain and strain rate. For the current study, the strain rate was nearly constant at 0.01/s. Since the flow stress at this strain rate is rather constant at given temperature, following values were used: σ_{eq}=17 MPa when T=550°C; and σ_{eq}=7.2 MPa when T=600°C [23].

EXPERIMENTAL SETUP

The experimental setup for the SPP is shown in Figure 1. The load and displacement of the upper ram were controlled and measured by the materials testing system (TestResources Inc, 800LE), while the temperature of the setup was controlled by the furnace (Applied Test System Inc).

The mean size of the Al6061 powder (Valimet, Inc.) used in this study was 13.82 μm. The alloy composition of the Al6061 powder is listed in Table 1. The die was fabricated with H13 tool steel and was heat treated to Rockwell hardness of HRC 50. The high temperature boron nitride spray (Momentive Performance Materials-Quartz, Inc.) was used to coat and lubricate the die wall and to prevent possible reaction between the aluminum and the die material at elevated temperatures.

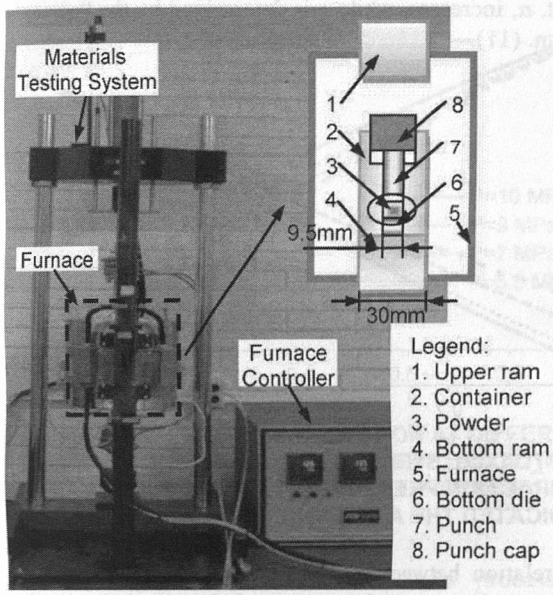

FIGURE 1: EXPERIMENTAL SETUP FOR SEMI-SOLID POWDER PROCESSING

TABLE 1: CHEMICAL COMPOSITION OF AL6061

Element	Al	Mg	Si	Cu	Fe	Cr	Zn	Mn	Ti
Amount (%)	Bal.	1.03	0.52	0.28	0.27	0.09	0.06	0.03	0.01

Three temperature settings, room temperature, 550°C and 600°C, were used in the experiments for the verification of the model. The liquid fraction at 600°C is about 7% according to the differential scanning calorimetry analysis conducted by Kim et al. [24]. The temperature profile for the experiment at 600°C is shown in Figure 2. The compaction at room temperature started with loosely stacked powder and continuously increased until 250 MPa. For the compaction at high temperatures, the powder was precompacted to 50 MPa at room temperature. After heating the material to the target temperature, the powder compact was compressed to a relative density above 0.95.

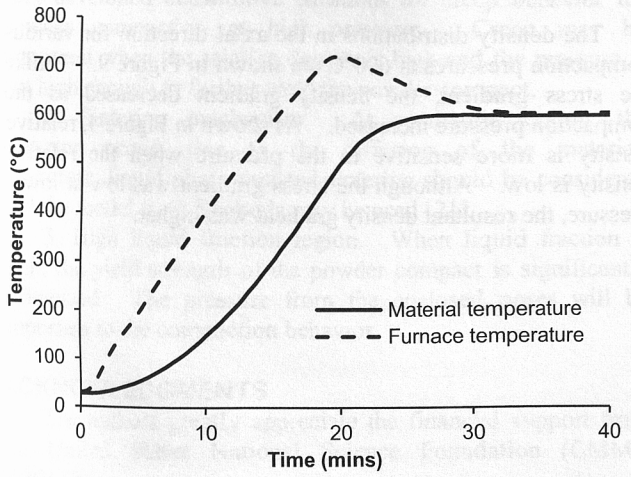

FIGURE 2: HEATING PROFILE USED IN THE EXPERIMENTS

RESULTS AND DISCUSSION

Compaction curve

The compaction curves at room temperature, 550°C and 600°C are shown in Figure 3 through Figure 5. The relative density of the parts was obtained from Archimedes' method. In Figure 3, the model prediction from the modified strain relation in Eqn. (8) for lower density matched the experimental results well, while the original relationship resulted in a slower density increase in the initial stage.

For the powder compacted at high temperature, an initial yield occurred because of the precompaction of the powder at room temperature. In Figure 3 and 4, the prediction of the initial yield conditioned matched the experimental data at both 550°C and 600°C.

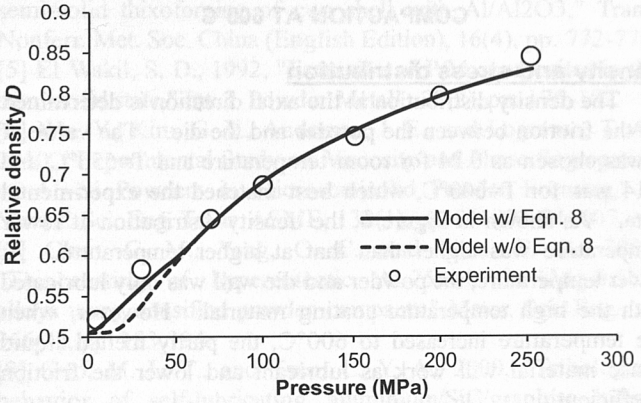

FIGURE 3: EXPERIMENT AND MODELING RESULTS FOR COMPACTION AT ROOM TEMPERATURE

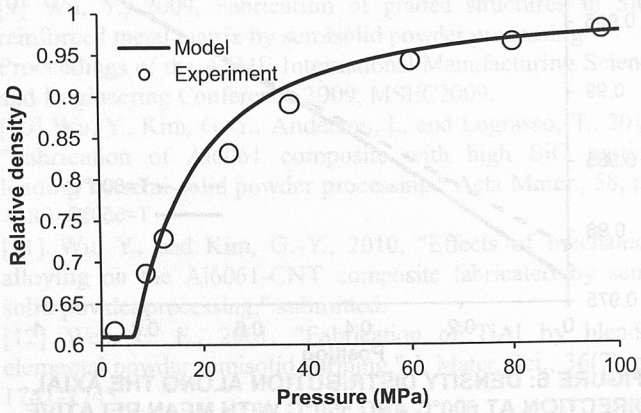

FIGURE 4: EXPERIMENT AND MODELING RESULTS FOR COMPACTION AT 550 °C

The liquid phase in the material significantly accelerated the consolidation of the powder compacts. As shown in Figure 5, the overall relative density of 0.95 was achieved when the solid relative density was only 0.88. On the other hand, 28 MPa of pressure was needed to compact the solid material to a relative density of 0.95 according to the model prediction.

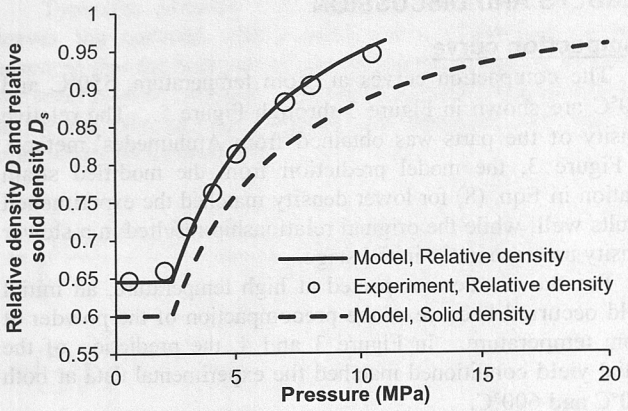

FIGURE 5: EXPERIMENT AND MODELING RESULTS FOR COMPACTION AT 600°C

Density and stress distribution

The density distribution in the axial direction is determined by the friction between the powder and the die. The value of μ was chosen as 0.24 for room temperature and T=550°C and 0.14 was for T=600°C, which best matched the experimental data. As shown in Figure 6, the density distribution at lower temperature was higher than that at higher temperature. At lower temperature, the powder and die wall was only lubricated with the high temperature coating material. However, when the temperature increased to 600°C, the partly melted liquid phase material will work as lubricant and lower the friction coefficient.

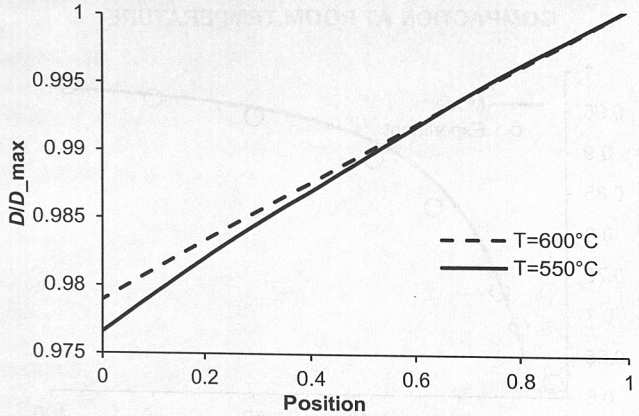

FIGURE 6: DENSITY DISTRIBUTION ALONG THE AXIAL DIRECTION AT 600°C AND 550°C WITH MEAN RELATIVE DENSITY OF 0.95. POSITION 1 INDICATED THE LOCATION AT THE PUNCH-POWDER INTERSECTION AND POSITION 0 INDICATED THE LOCATION AT THE BOTTOM DIE-POWDER INTERFACE.

The stress distribution in the axial direction at 600°C for different compaction pressure is shown in Figure 7. The stress distribution between the top and bottom of the powder compact increased as the pressure increased. According to Eqn. (10), the stress gradient increases as the stress transmission coefficient, α, increases, while α is determined by the Poisson's ratio in Eqn. (11).

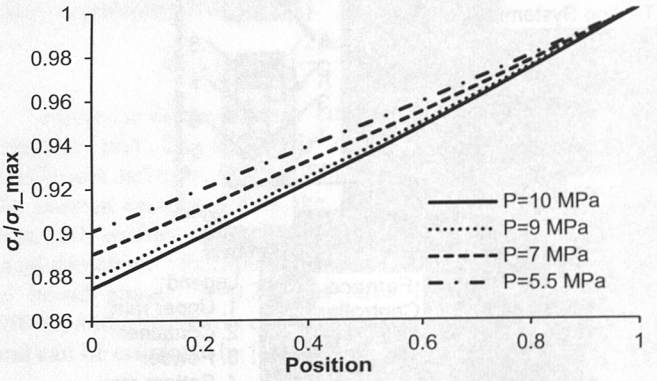

FIGURE 7: AXIAL STRESS DISTRIBUTION AT DIFFERENT COMPACTION PRESSURE. T=550°C AND σ_1_MAX INDICATED THE AXIAL STRESS AT POSITION 1.

The relation between the D_s and ν and α are shown in Figure 8. As the compaction pressure is increased, the density as well as the Poisson's ratio of the compact increases, resulting in an increase of the stress transmission coefficient. Therefore, the stress gradient increases with the increase in compaction pressure.

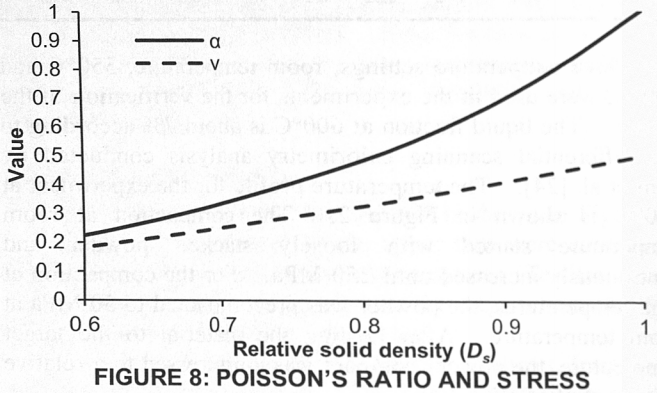

FIGURE 8: POISSON'S RATIO AND STRESS TRANSMISSION COEFFICIENT ESTIMATED WITH EQN. (11).

The density distributions in the axial direction for various compaction pressures at 600°C are shown in Figure 9. Unlike the stress gradient, the density gradient decreased as the compaction pressure increased. As shown in Figure 4, relative density is more sensitive to the pressure when the relative density is low. Although the stress gradient was low at lower pressure, the resultant density gradient was higher.

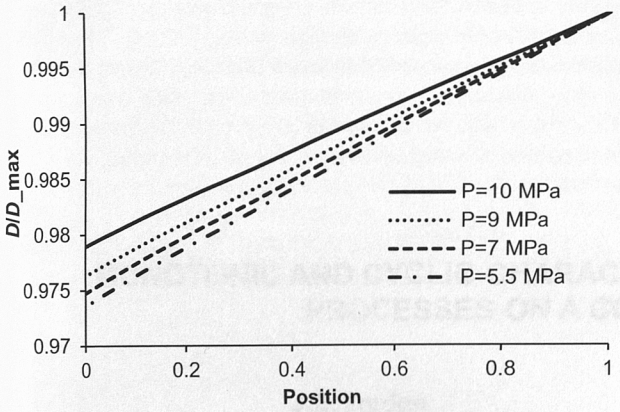

FIGURE 9: DENSITY DISTRIBUTION AT DIFFERENT COMPACTION PRESSURE. T=600°C AND *D_MAX* INDICATED THE DENSITY AT POSITION 1.

CONCLUSIONS

In this paper, the semi-solid powder processing was modeled for the first time, and the modeling results were compared with the experiments. The density and stress distribution during the powder compaction were analyzed. The results showed that the Shima-Oyane's model was capable of describing the compaction behavior of semi-solid materials. Consolidation in semi-solid range can significantly decrease the required pressure and time for full densification of the composite. The stress gradient in the axial direction was larger at higher compaction pressure, while the density gradient was smaller at higher pressure.

FUTURE WORK

In this study, SPP with relatively low liquid fraction of about 7% was investigated considering only plastic yielding during the consolidating of the powder compact. In the future, the following aspects will be considered:

1. Creep of material at high temperature. At high temperatures, the materials show creep behavior under pressure below the yield point [25]. Besson et al. [26] and Kuhn et al. [27] developed constitutive equations for creep behavior for powder compaction at high pressures. Creep may be important when the relative density is high and the pressure is not high enough to further yield the powder compact.

2. Sintering mechanism. At semi-solid region, the sintering occurs due to the diffusion of the material. Therefore, liquid phase assisted sintering should be considered and the model from Svoboda may be used [21].

3. High liquid fraction region. When liquid fraction is high, the yield strength of the powder compact is significantly influenced. The pressure from the enclosed pores will be important to the compaction behavior.

ACKNOWLEDGMENTS

The authors greatly appreciate the financial support from the United States National Science Foundation (CMMI-1030120).

REFERENCES

[1] Kim, G.-Y., Ni, J., Mayor, R., and Kim, H., 2007, "An experimental investigation on semi-solid forming of micro/meso-scale features," J. Manuf. Sci. Eng. Trans. ASME, 129(2), pp. 246-251.

[2] Kim, G.-Y., Koc, M., Mayor, R., and Ni, J., 2007, "Modeling of the semi-solid material behavior and analysis of micro-/mesoscale feature forming," J. Manuf. Sci. Eng. Trans. ASME, 129(2), pp. 237-245.

[3] Steinhoff, K., Weidig, U., and Weikert, J., 2004, "Micro semi-solid manufacturing - A new technological approach towards miniaturisation," Steel Res. Int., 75(8-9), pp. 611-619.

[4] Luo, S.-J., Cheng, Y.-S., and Wang, P.-X., 2006, "Pseudo-semi-solid thixoforging of cup shell with Al/Al2O3," Trans. Nonferr. Met. Soc. China (English Edition), 16(4), pp. 772-775.

[5] El Wakil, S. D., 1992, "Extrusion of P/M composites in the semi-solid state," Int. J. Powder Metall., 28(2), pp. 175-182.

[6] Wu, Y., Kim, G.-Y., Anderson, I. E., and Lograsso, T. A., 2010, "Experimental Study on Viscosity and Phase Segregation of Al--Si Powders in Microsemisolid Powder Forming," J. Manuf. Sci. Eng. Trans. ASME, 132(1), pp. 011003-011007.

[7] Chen, C. M., Yang, C. C., and Chao, C. G., 2004, "Thixocasting of hypereutectic Al-25Si-2.5Cu-1Mg-0.5Mn alloys using densified powder compacts," Mater. Sci. Eng., A, 366(1), pp. 183-194.

[8] Guo, M. L. T., and Tsao, C. Y. A., 2000, "Tribological behavior of self-lubricating aluminium/SiC/graphite hybrid composites synthesized by the semi-solid powder-densification method," Compos. Sci. Technol., 60(1), pp. 65-74.

[9] Wu, Y., 2009, Fabrication of graded structures in SiC-reinforced metal matrix by semisolid powder processing Proceedings of the ASME International Manufacturing Science and Engineering Conference 2009, MSEC2009.

[10] Wu, Y., Kim, G.-Y., Anderson, I., and Lograsso, T., 2010, "Fabrication of Al6061 composite with high SiC particle loading by semi-solid powder processing," Acta Mater., 58, pp. 4389-4405.

[11] Wu, Y., and Kim, G.-Y., 2010, "Effects of mechanical alloying on the Al6061-CNT composite fabricated by semi-solid powder processing," submitted.

[12] Wen, C. E., 2001, "Fabrication of TiAl by blended elemental powder semisolid forming," J. Mater. Sci., 36(7), pp. 1741-1745.

[13] Yasue, K., 2000, "Elemental blended powders semisolid forming of Ti-Al based alloys," J. Mater. Sci., 35(23), pp. 5927-5932.

[14] Young, R. M. K., and Clyne, T. W., 1986, "A powder-based approach to semisolid processing of metals for fabrication of die-castings and composites," J. Mater. Sci., 21(3), pp. 1057-1069.

[15] Brewin, P. R., Coube, O., Doremus, P., and Tweed, J. H., 2008, Modelling of powder die compaction, Springer, London.

[16] Lee, S. C., and Kim, K. T., 2002, "Densification behavior of aluminum alloy powder under cold compaction," Int J Mech Sci, 44(7), pp. 1295-1308.
[17] Fleck, N. A., Kuhn, L. T., and Mcmeeking, R. M., 1992, "Yielding of Metal-Powder Bonded by Isolated Contacts," J Mech Phys Solids, 40(5), pp. 1139-1162.
[18] Kwon, Y. S., Lee, H. T., and Kim, K. T., 1997, "Analysis for cold die compaction of stainless-steel powder," J Eng Mater-T Asme, 119(4), pp. 366-373.
[19] Shima, S., and Oyane, M., 1976, "Plasticity Theory for Porous Metals," Int J Mech Sci, 18(6), pp. 285-291.
[20] Kang, C. G., and Jung, H. K., 1999, "Finite element analysis with deformation behavior modeling of globular microstructure in forming process of semi-solid materials," Int J Mech Sci, 41(12), pp. 1423-1445.
[21] Svoboda, J., Riedel, H., and Gaebel, R., 1996, "A model for liquid phase sintering," Acta Mater., 44(8), pp. 3215-3226.
[22] Hatch, J. E., 1984, Aluminum: Properties and physical metallurgy, American Society for Metals, Metals Park, Ohio.
[23] Lou, B. Y., Huang, J. C., Wang, T. D., and Langdon, T. G., 2002, "Flow behaviour of aluminium-based materials at ultrahigh temperatures in the presence of a liquid phase," Mater Trans, 43(3), pp. 501-509.
[24] Kim, W. Y., Kang, C. G., and Kim, B. M., 2007, "The effect of the solid fraction on rheological behavior of wrought aluminum alloys in incremental compression experiments with a closed die," Materials Science and Engineering: A, 447(1-2), pp. 1-10.
[25] Harper, J., and Dorn, J. E., 1957, "Viscous Creep of Aluminum near Its Melting Temperature," Acta Metall., 5(11), pp. 654-665.
[26] Besson, J., and Abouaf, M., 1992, "Rheology of Porous Alumina and Simulation of Hot Isostatic Pressing," J. Am. Ceram. Soc., 75(8), pp. 2165-2172.
[27] Kuhn, L. T., and Mcmeeking, R. M., 1992, "Power-Law Creep of Powder Bonded by Isolated Contacts," Int J Mech Sci, 34(7), pp. 563-573.